Accurate atomistic first-principles calculations of electronic stopping

André Schleife,[1,*] Yosuke Kanai,[1,2,†] and Alfredo A. Correa[1,‡]

[1]*Quantum Simulations Group, Lawrence Livermore National Laboratory, Livermore, California 94550, USA*

[2]*Department of Chemistry, The University of North Carolina at Chapel Hill, Chapel Hill, North Carolina 27599-3290, USA*

(Received 24 July 2014; published 20 January 2015)

We show that atomistic first-principles calculations based on real-time propagation within time-dependent density functional theory are capable of accurately describing electronic stopping of light projectile atoms in metal hosts over a wide range of projectile velocities. In particular, we employ a plane-wave pseudopotential scheme to solve time-dependent Kohn-Sham equations for representative systems of H and He projectiles in crystalline aluminum. This approach to simulate nonadiabatic electron-ion interaction provides an accurate framework that allows for quantitative comparison with experiment without introducing *ad hoc* parameters such as effective charges, or assumptions about the dielectric function. Our work clearly shows that this atomistic first-principles description of electronic stopping is able to disentangle contributions due to tightly bound semicore electrons and geometric aspects of the stopping geometry (channeling versus off-channeling) in a wide range of projectile velocities.

DOI: 10.1103/PhysRevB.91.014306 PACS number(s): 61.80.−x, 34.20.−b, 34.50.Bw

I. INTRODUCTION

A fast particle (referred to as "projectile" in the following) entering into a target material ('host') produces effects on a wide range of length and time scales. For fast projectiles, the dominant phenomenon at initial stages is stopping due to interactions with electrons of the host (electronic stopping), which is the main topic of this paper. Later stages involve secondary knocked atoms, track formation, and melting, as well as long-term irreversible effects on the material that are jointly referred to as radiation damage [1–4]. Understanding those interactions is highly important for fusion and fission applications [5], high-energy density physics [6], medicine [7], as well as nuclear safety [8].

On average, the stopping power of a material for a given type of projectile is characterized by the projectile's velocity. Conceptually, the stopping phenomenon is divided into two categories depending on the type of excitation produced: (i) at low projectile velocities, the dominant effect is the nuclear stopping that mainly has the effect of displacing the host's nuclei, which causes lattice excitations; (ii) at high projectile velocities, nuclei do not have enough time to react and absorb energy or momentum; instead, electronic excitations are by far more important, thus becoming the main channel for energy dissipation of the projectile. At even higher velocities, also the response time of electrons is limited, and thus there exists a maximum also in the electronic stopping curve.

While nuclear stopping can be understood in a classical picture of lattice vibrations and displaced atoms (as typically handled by molecular dynamics or collision models) [9,10], electronic stopping presents additional challenges due to its quantum mechanical nature. A fully atomistic first-principles framework for the calculation of electronic stopping is desirable as it enables quantitative investigations of complex materials, compounds of arbitrary stoichiometry, and geometry (such as thin films, alloys, superlattices, nanostructures), different phases (liquids, halotropes) and densities, and ultimately by-design materials. Such systematic capability of first-principles simulations would allow studying scenarios that cannot be captured by empirical-based approaches typically used nowadays [11,12].

Ever since the phenomenon of electronic stopping was discovered, a number of approximations and models were conceived: the classical Coulomb scattering formulas of Rutherford [13], Thomson [14], and Darwin [15], the quantum-oscillator strength formula by Bethe [16–18], electron gas models by Fermi and Teller [19], and the general linear-response treatment by Lindhard (see Refs. [20–22] and references therein). Nonperturbative calculations (necessary to model, e.g., the Barkas effect [23] and the Z_1 oscillations) of the electronic stopping in the uniform electron gas started in the 1980's by Echenique *et al.* [24] with the advent of explicit electronic orbital methods [25] and their time-dependent counterparts [26]. However, those still require *ad hoc* assumptions and separate theories regarding the charge state of the projectile or the number of participating host electrons that take part in the stopping process [27]. For a historical review of theoretical approaches to electronic stopping see Ref. [28].

In the past few decades, both rapidly advancing supercomputers and modern electronic-structure methods made it possible to calculate key parameters of analytical models directly from first principles. Parameter-free models go significantly beyond effective theories as they provide detailed information about dependencies on projectile direction and initial conditions, specific effects of defects, nonadiabatic forces [29,30], and electron-hole or plasmon excitation. A fully atomistic first-principles calculation of electronic stopping for a wide range of projectile velocities and especially around the maximum of the electronic stopping curve, however, has remained elusive. Only recently, the possibility of quantitatively describing the interaction of projectile atoms with the electronic *and* ionic system of the host material entirely within first-principles calculations has come within reach [30–37]. These recent advances for realistic materials rely on nonperturbative time-dependent density functional theory (TDDFT) [26],

*schleife@illinois.edu
†ykanai@unc.edu
‡correaa@llnl.gov

and its implementation in efficient electronic-structure codes [38,39].

At this point, however, there are still many open questions regarding, not only the physics of electronic stopping (e.g., related to the number of explicitly "participating" host electrons, degree of ionization of the projectile, impact geometry), but also the numerics (e.g., convergence of basis sets and finite-size effects) and their interplay. As discussed in the recent review by Race *et al.* [28] and by the authors themselves [30], existing state-of-the-art first-principles calculations of electronic stopping power still suffer convergence issues, some of which may be responsible for discrepancies between calculations and experimental results [30,34]. In addition, the physics of the stopping process itself deserves further attention, and it is important to take into account stopping geometry and identifying the participating electronic states. For this reason, this work aims at simulating directly and accurately the electronic stopping for a wide range of projectile velocities ($0 < v \leqslant 8$ atomic units, at. u.). We address this issue in a systematic way by applying our new large-scale implementation [39,40] of real-time TDDFT using a plane-wave basis to the case of light projectiles (hydrogen/proton, helium/α particle) in bulk aluminum. These particular examples allow us to establish an essential set of requirements, both numerically and theoretically, for a first-principles calculation to reach experimental accuracy for the *entire range* of projectile velocities. In particular, this allows us to unravel the connection between off-channeling trajectories and contributions to electronic stopping from localized, strongly bound semicore electrons. Further, we investigate the interesting case of He, which is interesting because the He projectile can assume several ionization states. We also explicitly discuss the influence of the charge state by studying both H^+ and He^{2+} projectiles.

The remainder of this work is structured as follows. In Sec. II, we briefly outline the theoretical approach and discuss numerical aspects. In Secs. III and IV, we discuss the difference in stopping for channeling and off-channeling hydrogen and helium projectiles in aluminum, respectively, highlighting the influence of semicore electrons, as well as different initial conditions (ion versus neutral atom). These quantitative analyses provide detailed insights into the complex physics related to the charge state and bound states of the projectile atom as well as the influence of the stopping geometry. Section V summarizes and discusses future directions.

II. THEORETICAL AND COMPUTATIONAL APPROACH

The method used to calculate electronic stopping in this work follows that of Pruneda *et al.* [34] and consists of a discrete time-integration of the time-dependent Kohn-Sham (TD-KS) equations [41,42],

$$\mathrm{i}\hbar\frac{\partial}{\partial t}\phi_i(\mathbf{r},t) = \left\{-\frac{\hbar^2\nabla^2}{2m} + \hat{V}_{\mathrm{ext}}(t) + V_{\mathrm{s}}[n(t)](\mathbf{r})\right\}\phi_i(\mathbf{r},t). \tag{1}$$

In Eq. (1), $\mathbf{r}$ is the spatial coordinate and t is time. $V_{\mathrm{s}}[n(t)](\mathbf{r})$ describes electrostatic (Hartree) electron-electron interaction and quantum-mechanical exchange-correlation (XC) potential for which we use the adiabatic local-density approximation (ALDA) [43,44]. The (time-dependent) potential acting on the electrons, $\hat{V}_{\mathrm{ext}}$, is given by the ionic system (including local and nonlocal parts of the pseudopotentials) and its time-dependence is that of the fast-moving projectile. Real-time propagation requires the specification of an initial condition for (i) the host nuclei (defined by the equilibrium structure of the material) as well as position and velocity vector of the projectile, and (ii) the electronic state (KS states and electron density) that is obtained here through solving the ground state (time-independent) KS equations for the initial atomic positions.

Regarding (ii), in this work we study two different initial charge states of the projectile to investigate the dependence of electronic stopping. In one case, we use an initial condition that represents "neutral" (or screened) projectiles from the solution of the static KS equations with the projectile included in the external potential. In the other case, we introduce an alternative approach to treat charged projectiles: the initial condition is set up by the ground-state solution of the KS equations for the pristine host material without any projectile, later the fully ionized atom (e.g., H^+ or He^{2+}) is added in the first step of the time integration, producing a sudden change in the (external) potential. Note that in both cases, we only control the initial state and not the subsequent dynamics which is given by the TD-KS equations. The initial state of a fully ionized projectile might be more realistic for fast ions as it is closer to the charge state after reaching the dynamical steady state described in Ref. [45].

We have recently developed a general purpose TD-KS explicit time-integration scheme for performing real-time TDDFT and Ehrenfest molecular dynamics simulations within a pseudopotential plane-wave framework and described its implementation in detail in Ref. [39] based on the QBOX code [46]. Thanks to the ability of systematically converging the plane-wave basis this overcomes basis-size, limitations of earlier approaches [30]. Additionally, our implementation scales very well up to large numbers of processors (excellent scaling on up to 1 million computer cores [40]), allowing us to consider large simulation cells and to study and eliminate the finite-size error in the simulations.

To compute electronic stopping, we use the time-dependent energy $E(t)$,

$$E(t) = \sum_i \int d\mathbf{r}\phi_i^*(\mathbf{r},t)\left[\frac{-\hbar^2\nabla^2}{2m} + \hat{V}_{\mathrm{ext}}(t)\right]\phi_i(\mathbf{r},t) + E_{\mathrm{s}}[n(t)] + V_{\text{ion-ion}}(t), \tag{2}$$

which comprises of the electronic kinetic energy, the external (electron-ion) potential $\hat{V}_{\mathrm{ext}}(t)$, the electron-electron interaction $E_{\mathrm{s}}[n(t)]$ (Hartree interaction and XC density-functional approximation), and the configurational energy $V_{\text{ion-ion}}(t)$. The external potential is handled in the pseudopotential approximation as it is customary in plane-wave schemes. E reported here is the *total* energy $E_{\mathrm{total}}(x)$ minus the kinetic energy of the ion(s), which converges toward the adiabatic energy in the limit of low atom velocity. Note that the terms that are purely a function of ion coordinates do not contribute to the definition of electronic stopping power because they are (quasi)periodic in long trajectories. $E(t)$ changes as a function of the projectile position $x(t)$, while integrating the TD-KS

equations in time [34], since the projectile deposits energy into the electronic system as it moves through the host. The increase of E as a function of projectile displacement x allows us to determine the instantaneous stopping power

$$S(x) = dE(x)/dx. \quad (3)$$

$S(x)$ has the dimension of a force (E_H/a_B) and can also be understood as a "drag force" acting on the projectile. In Ref. [47], we show in detail that the plane wave cutoff energy of 50 Ry and the integration time step $\Delta t = 0.35$ as (attoseconds) introduce only a very small error of less than $10^{-2} E_H/a_B$; and that the plane wave basis used here is fully converged even for large projectile velocities and that computing the electronic stopping from Eq. (3) or directly using the Hellman-Feynman force acting on the projectile are equivalent as long as the convergence criteria are met.

A. Averaged versus instantaneous electronic stopping: Channeling geometry

Equation (3) defines the *instantaneous* electronic stopping $S(x)$ as a function of the projectile's position in the host material. In order to compare to experiment, it is necessary to compute a meaningful "average" value. Such an average has both temporal and spatial character. In this work, we propose an averaging strategy by invoking two different stopping geometries: (i) channeling projectiles that travel through the host without approaching the host atoms too closely [(also called *hyperchanneling* if high-symmetry channels are used]; in this work, we restrict the discussion to a [100] channel, cf. inset of Fig. 1); and (ii) off-channeling projectiles, which are approximated here by choosing a random (i.e., incommensurate with the crystal's symmetry) direction for the projectile to travel through the host material. The stopping geometry is expected to have a significant impact on the calculated electronic stopping because the charge density in the close vicinity of host atoms is larger and, hence, the interaction of the projectile with this electronic charge density is expected to be stronger.

In Fig. 1, the instantaneous electronic stopping is shown for different velocities of the hydrogen projectile in aluminum for the channeling condition. For projectiles faster than 1.0 at.u., the figure shows a "kink" in the beginning of the simulation, which we interpret as a transient produced by the initial sudden motion of the projectile. The amplitude of this kink depends on the projectile velocity, but the spatial extent of the kink in the cell does not, and is always restricted to $x \leqslant 5\ a_B$.

In addition, it can also be seen that for large velocities (e.g., $v = 6.0$ at. u. in Fig. 1) the stopping starts to deviate from the steady behavior within the first supercell as soon as the projectile re-enters the periodic image of the simulation cell. These effects occur because the projectile effectively interacts with nonequilibrium electrons on the same channel. This deviation is stronger for faster projectiles and smaller supercells. For this reason, re-entering on the same path should be avoided and a large enough simulation cell needs to be used. In the present work we use a simulation cell of 256 atoms (cubic lattice constant of 4.05 Å) to compute converged results for the electronic stopping which, at the same time, allows using only the Γ point for sampling the Brillouin zone.

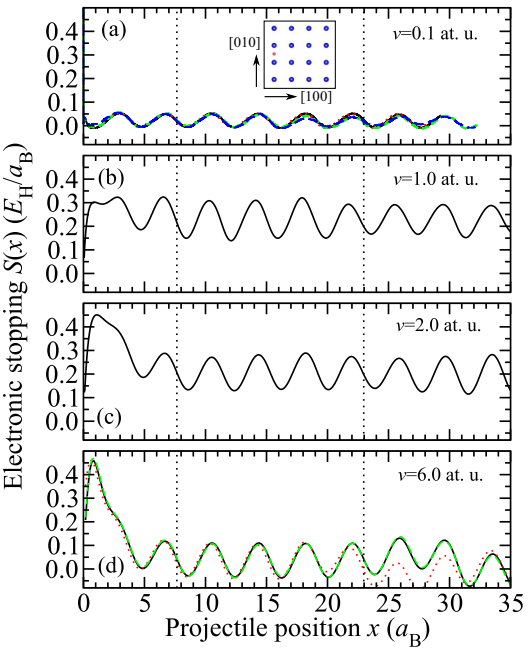

FIG. 1. (Color online) Instantaneous electronic stopping (in E_H/a_B) from Eq. (3) for hydrogen projectiles of different velocities in aluminum. Black solid lines were obtained for a (30.62×30.62×30.62) a_B^3 supercell (256 atoms), red dotted lines for a (22.97×30.62×30.62) a_B^3 supercell (192 atoms), green dashed lines for a (30.62×22.97×22.97) a_B^3 supercell (144 atoms), and blue dashed lines for a (22.97×22.97×22.97) a_B^3 supercell (108 atoms). The region in between the dotted vertical lines is used to extract the stopping. The inset shows the projectile (small circle) in part of the supercell of aluminum atoms (big circles).

For computing the averaged electronic stopping, we need to exclude both the influence from the initial kink as well as the effects of re-entering the simulation cell on the same path. In addition, since we are interested in the electronic stopping as an entirely nonadiabatic effect that cannot be captured within the adiabatic Born-Oppenheimer approximation, we would need to subtract the oscillations of $dE(x)/dx$ that result from the periodic lattice (see Fig. 1) when averages are not computed over entire lattice periods. Instead of computing these quantities in a separate Born-Oppenheimer (ground-state) simulation we pursue a different route: we integrate $S(x)$ over several lattice periods indicated by the vertical dotted lines in Fig. 1, and divide by the corresponding distance. Since we are using entire lattice periods, the integral over the same quantity in a Born-Oppenheimer simulation would yield exactly zero, as all electrons remain in their ground state at all times and points are equivalent.

B. Averaged versus instantaneous electronic stopping: off-channeling geometry

In general, there are many different possible trajectories for off-channeling projectiles. As discussed above, it can be expected that the instantaneous electronic stopping for the projectile very close to host atoms differs significantly from the one for the projectile far from host atoms. There are various possible ways to explore these conditions, for example,

by repeating and averaging simulations at different impact parameters [37,48].

In order to circumvent, the computational cost associated with carrying out calculations for a large number of trajectories and computing weighted averages from those, we propose to compute instead one long trajectory (about ten times as long as for channeling projectiles discussed above) for the projectile moving through the host material in a *random* direction (incommensurate with the crystal symmetry) at a given velocity. This approach is more appealing than alternative off-channeling strategies because: (i) one single (long) simulation is, in principle, enough to sample *all* possible impact parameters, (ii) different impact parameters are sampled with weights that are geometrically correct, (iii) head-on or near-head-on collisions are rather rare but important events that contribute to the stopping accordingly. Even though the projectile traveling on a random direction can approach host atoms very closely, those will not be displaced since we keep the velocities of *all* atoms constant in our simulations (any remnant ionic stopping contributions are removed this way). In other words, we replace a geometric average by a time average that can be performed in a single simulation run. Since the projectile does not re-enter the simulation cell on the same path each time, re-entering does not influence the results as much as we observed for the channeling projectile. We verified that this approach is independent of the particular choice of the random direction (as long as those are incommensurate with respect to the lattice vectors) by comparing two different trajectories.

We now address how to compute the average of the electronic stopping from the instantaneous stopping in the off-channeling random case. The resulting curves for E are depicted in Fig. 2(a) and clearly show pronounced peaks (for when the projectile is very close to a host atom) as well as smoother parts. We note that in regions of low electron density (far from host atoms) the instantaneous stopping agrees with that of the channeling conditions. However, when the projectile passes a host atom at short distance we observe *unsymmetrical* peaks and overall steplike contributions to the stopping (with sudden increases of the slope). We then compute average slopes of the curves for E in Fig. 2(a) by linear least-squares fits to the data starting at $x = 6\,a_B$ (the initial "kink" is omitted for the fitting) and ending at a maximum value x. In Fig. 2(b), we show the convergence of the *running* average slope from the fit with respect to the maximum value x. This plot shows the high level of accuracy that we can reach by converging this average slope, which *a posteriori* justifies our approach to simulate off-channeling trajectories.

C. Effect of semicore electrons and pseudopotential Radii

In order to reduce the computational effort, pseudopotentials are used to describe the electron-ion interaction [V_{ext} in Eqs. (1) and (2)]. The atom-centered pseudopotential takes the form of a local smooth potential plus a separable Kleinman-Bylander nonlocal operator [49],

$$\langle \mathbf{r}'|\hat{V}_{\text{ext}}|\mathbf{r}\rangle = V_{\text{local}}(\mathbf{r})\delta(\mathbf{r}'-\mathbf{r}) + \sum_{\ell m} \frac{\langle \mathbf{r}'|\psi^{\text{PS}}_{\ell m}\delta V_\ell\rangle\langle\delta V_\ell \psi^{\text{PS}}_{\ell m}|\mathbf{r}\rangle}{\langle\psi^{\text{PS}}_{\ell m}|\delta V_\ell|\psi^{\text{PS}}_{\ell m}\rangle}. \tag{4}$$

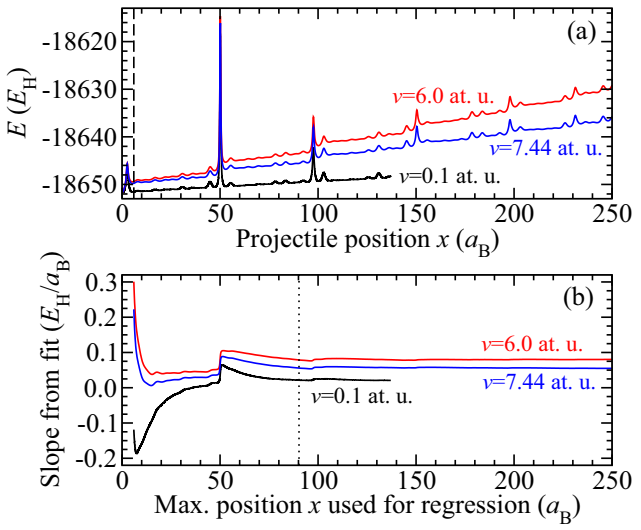

FIG. 2. (Color online) In (a), the electronic total energy for a hydrogen projectile on an off-channeling (random) trajectory in aluminum is shown for $v = 0.1$ (black), 6.0 (red), and 7.44 (blue). In (b), the slopes of linear least-squares fits between $x_1 = 6\,a_B$ and a given maximum position x is shown as a function of this maximum position. The "kink" between x=0 a_B and 6 a_B [indicated by the vertical dashed line in (a)] is omitted for the fitting. The vertical dotted line indicates the (converged) average value that we used for the discussion of electronic stopping.

The second term is nonzero inside each atomic sphere centered at each atom, while the first term coincides with a local Coulomb potential outside the sphere. In a pseudopotential scheme such as the one used in this work, the pseudopotential spheres (defined by a cutoff radius when constructing the pseudopotential) of the projectile and the host atom will overlap when the projectile is very close to a host atom, for instance, in the off-channeling geometry. Since we are not interested in the exact value of the energy during the close encounter but only the increase of E over time, this overlap is not as serious as in the case of static total-energy calculations. In this work, we simply consider the event of sphere overlap as part of the dynamics that is, although temporarily unrealistic, still acceptable in terms of connecting the initial state (before the overlap) to a final state (after the overlap). We confirmed that the influence of the sphere radius on the result for electronic stopping is small by running test calculations with pseudopotentials that we created for different sphere radii. To this end, using the OPIUM code [50], we prepared different Troullier-Martins norm-conserving pseudopotentials [51] for aluminum with three electrons ($3s^2 3p^1$) as well as 11 electrons ($2s^2 2p^6 3s^2 3p^1$) in the valence shell (explicit in the supercell calculation). This variety of pseudopotential choices allowed us to systematically explore effects due to semicore electrons, which we find crucial to obtaining accurate results for a wide range of projectile velocities (as discussed below).

III. HYDROGEN AND PROTON PROJECTILE IN ALUMINUM

In this work, we use the case of a hydrogen projectile in aluminum to systematically study the physics of electronic

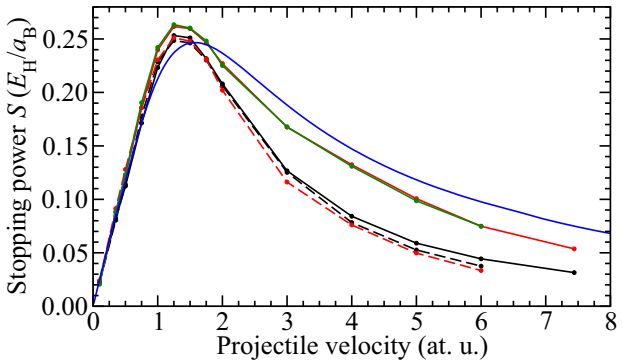

FIG. 3. (Color online) Electronic stopping calculated as a function of the velocity of a hydrogen projectile in aluminum. The solid blue curve represents experimental results provided by the SRIM table [52]. Dashed (black and red) curves were computed treating the $3s^2 3p^1$ electrons of aluminum as valence electrons. Solid (black, red, and green) curves were computed including also the $2s^2 2p^6$ electrons in the valence shell. Black curves represent hyper-channeling and red curves correspond to off-channeling projectiles. The solid green line corresponds to the H^+ charge state (proton) of the projectile.

stopping in this representative system, and also to address key numerical aspects of the first-principles theoretical framework. The comparison with perturbative theory is better justified for the hydrogen projectile than for other projectiles; and the stopping geometry as well as convergence aspects of the problem can be characterized with more exhaustive detail. We compare our results to the empirically fitted SRIM results, as an accurate summary and average of numerous experiments [11], as well as other experimental [53] and theoretical works [22,30,54].

Figure 3 shows our calculated results for channeling as well as off-channeling projectiles in different charge states and for different valence-electron configurations. We start by comparing results for channeling projectiles to off-channeling ones with only $3s^2 3p^1$ electrons treated as valence states in the aluminum pseudopotential. The corresponding black and red dashed curves in Fig. 3 are very close to each other, showing that the stopping geometry is practically irrelevant in this case. While the agreement of both curves with the SRIM curve is excellent for the linear part up to a velocity of $\approx$1 at. u., we observe an increasing underestimation for faster projectiles, i.e., past the maximum of electronic stopping.

Next, we compare channeling and off-channeling stopping including also $2s^2 2p^6$ electrons explicitly in the valence shell of aluminum in addition to $3s^2 3p^1$ electrons. Figure 3 clearly shows that the result barely changes for channeling hydrogen when these semicore electrons are treated explicitly as valence electrons (solid black curve). However, as shown by the red solid curve in this figure, the situation is vastly different for off-channeling hydrogen: this case agrees well with others up to a projectile velocity of $\approx$1 at.u., but the electronic stopping is significantly higher for faster projectiles. This now closely agrees with SRIM data over the entire velocity range of the projectile.

These aspects point to two important results regarding the physics of electronic stopping: (i) in order to reproduce experimental data for electronic stopping power over a wide range of projectile velocities, it is not sufficient to consider only channeling projectiles. This result is further corroborated by experiments, performed under very controlled conditions (mono-crystalline samples and specifically oriented setup), reporting that electronic stopping for channeling projectiles can be smaller by a factor two or more [55]. (ii) For stopping geometries where the projectile closely approaches the nuclei of the host material (as in the off-channeling case studied in this work), it is important to account for (semi-) core electrons of the host material in the calculations. This means that not only the outermost valence electrons participate in the stopping of the projectile, but also those (semi-) core electrons contribute significantly. Conversely, we also show that if the projectile does not closely encounter nuclei on its trajectory through the host material, only the valence electrons of the host are involved in the stopping.

In addition, Fig. 3 shows a comparison of an initial condition corresponding to the neutral hydrogen atom (red solid curve) as well as the (positively charged) proton (green solid curve). These two cases yield the same result for electronic stopping, indicating that charge equilibration of the projectile happens on very short time scales in metals, and this is consistent with the fact that a hydrogen atom does not hold bound states in aluminum [45].

In order to understand the observed behavior in more detail, we compare our first-principles results to analytical calculations of electronic stopping within linear-response theory based on the Lindhard dielectric function for a uniform electron gas of a given effective density [21]. We evaluate the stopping as $S = 2Z_1^2 e^2/(\pi v^2) \times L(v,n)$, where L is the stopping number, a double integral in frequency (energy) and wave number (momentum) of the electron-energy loss function in the RPA for the uniform electron gas:

$$L(v,n) = \int_0^\infty \frac{dk}{k} \int_0^{kv} d\omega\omega\, \Im[\varepsilon_{\mathrm{RPA}}(n,k,\omega)^{-1}]. \qquad (5)$$

Although our TDDFT method goes beyond this linear approximation, the comparison in Fig. 4 is helpful for interpreting our results. In order to investigate the influence of (semi-) core electrons, different densities of the electron gas are assumed, corresponding to three, nine, and 11 valence electrons of the host atoms. It is remarkable that, for projectile velocities larger than 1.5 at.u., the analytical results assuming 3 valence electrons coincide with the curve that we computed for a *channeling* projectile (cf. Fig. 4). This reaffirms that in the channeling geometry only the outermost three valence electrons of aluminum contribute to the electronic stopping, as discussed above. However, we also point out that the two curves disagree for low projectile velocities, which indicates that the analytical Lindhard model is not able to capture all aspects of electronic stopping even for the simple case of a channeling trajectory. We would like to note that more sophisticated approaches, based on the dielectric response including the exact many-body and dynamic exchange-correlation treatment for low velocity projectiles, are available in the literature [56,57]. In the context of the present work, using current-density functional theory [58] is particularly promising for future extensions, since the currents generated might be of significance.

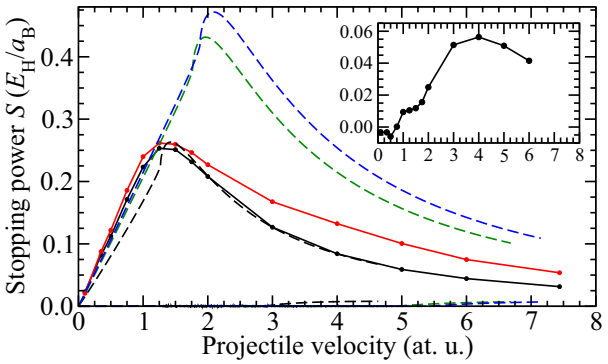

FIG. 4. (Color online) Electronic stopping calculated as a function of the velocity of a hydrogen/proton projectile in aluminum. Solid curves were computed for aluminum host material with $2s^2 2p^6 3s^2 3p^1$ electrons in the valence shell for channeling (black) and off-channeling (red) projectiles. Dashed curves are computed using the Lindhard dielectric function for three valence electrons (black), nine valence electrons (green), and 11 valence electrons (blue) per aluminum atom. Finite-size errors due to finite plasmon wavelength in the supercell are estimated within the Lindhard model and indicated at the bottom of the figure. The inset shows the electronic stopping difference between the curves with and without semi-core electrons for off-channeling projectiles.

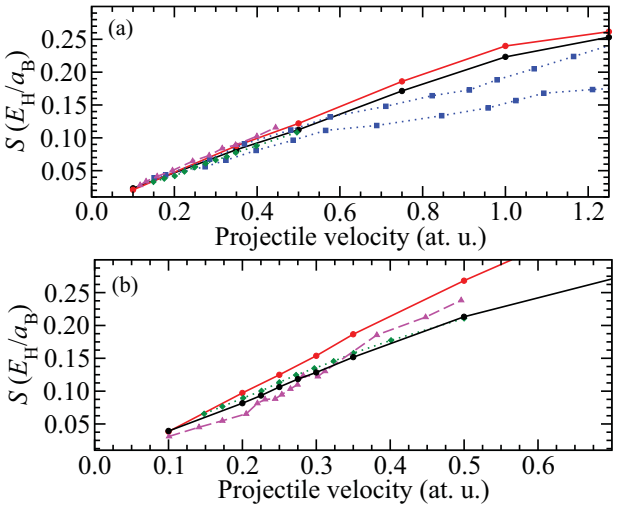

FIG. 5. (Color online) Electronic stopping of H (a) and He (b) projectiles in Al: solid (black and red) curves were computed including $2s^2 2p^6$ electrons in the valence shell. Black curves represent hyper-channeling and red curves correspond to off-channeling projectiles. Dotted blue results are calculated results from Ref. [30], dotted green are from Ref. [54], and dashed magenta curves represent experimental data (Ref. [53]). A larger Δt of 0.69 as was used for the channeling trajectory of He in Al.

For comparison, Fig. 4 also shows that the stopping from the linear response (assuming nine and 11 valence electrons) overestimates the stopping for a fast projectile. We trace this observation back to the fact that the core electrons contribute to electronic stopping only partially. However, the faster the projectile, the closer those curves become, which indicates that increasingly more core electrons play a role (at the same time that linear response becomes a better approximation).

The characteristic velocity at which electrons in semicore states start to play a role in off-channeling trajectories is depicted in the inset of Fig. 4. In our calculations, the lower-lying semicore electrons of aluminum are separated by about 66 eV from the lowest empty conduction states. The approximate minimum velocity required for a projectile to excite electrons across this gap, which is also compatible with conservation of total momentum is given by $v^* \approx \Delta/(2\hbar k_F)$. Using this separation as an effective "band gap" (in a system with crystalline symmetry system the argument is only approximate), the corresponding estimated onset for stopping coincides with where the curve for channeling and off-channeling projectiles start to deviate, around $v^* = 0.85$ at.u. (cf. inset of Fig. 4), in approximate agreement with the simulation result.

We also used the analytical model based on linear response theory to estimate a possible finite-size error in our first-principles calculations, because plasmons with wave lengths longer than the simulation cell cannot be captured correctly in supercell simulations. In order to estimate this error, we calculate the electronic stopping using the Lindhard formula by cutting off the momentum integration in Eq. (5) at a wave number that corresponds to the simulation cell size ($k_{cut} \simeq \pi/L$). The difference to the fully converged integral is plotted in Fig. 4, and shows that finite-size error (for the 256-atom supercell used here) is negligible even for projectile velocities well beyond the stopping curve maximum.

Finally, in Fig. 5(a), we compare our results for channeling as well as off-channeling projectiles to experimental [53] and other theoretical [30,54] results, finding very good agreement with measurements [53]. The experimental electronic stopping is only slightly larger: the curve corresponding to the channeling projectiles is within approximately 12% (or better) of the experimental result for velocities between 0.1 and 0.45 at.u., and the off-channeling curve is within approximately 6% (or better) of the experimental values. For another recent calculation of electronic stopping of hydrogen projectiles in aluminum [30] based on a similar framework, the agreement with experiment is poorer in the same velocity range. More importantly, Ref. [30] reports significantly smaller values for the stopping for $v > 0.6$ at.u. when comparing their channeling or their off-channeling trajectory to ours. This may be attributed to the local-orbital basis and size effect limitations as described therein. The work by Zeb *et al.* [54] uses the same framework as Ref. [30] to study a channeling projectile in aluminum and their results are very close to ours in the low velocity limit. However, we emphasize that our new curves for an off-channeling projectile agree with experimental data (SRIM curve) in the *entire range* of projectile velocities.

To provide further details of the participation of the semicore levels, we explore how the energy of the individual electrons (rather than the total energy) varies due to the projectile motion. This allows us to nominally disentangle the effect of the passing projectile into different valence and semicore electron contributions. We calculate the expectation value of the instantaneous TDKS Hamiltonian on the TDKS orbitals, and given that the different electronic states are well

TABLE I. Stopping contributions due to the valence ($n = 3$) as well as semicore ($n = 2$) electrons, estimated from the time-dependent expectation values for two different projectile velocities and for channeling as well as off-channeling trajectories of H in Al.

	v	$n = 3$	$n = 2$
channeling	1.0 at. u.	93.3%	6.7%
	3.0 at. u.	95.0%	5.0%
off-channel	1.0 at. u.	87.3%	12.7%
	3.0 at. u.	76.0%	24.0%

separated in terms of their energy, we can at least identify three separate bands corresponding to electrons with different valence ($n = 3$) and semicore ($n = 2$) character. In the same way that the sum of the expectation energy values is not the total energy of the system [39], the sum of the drifts of the individual energies is not exactly the total energy drift (i.e., the electronic stopping). However, the variation of a partial sum of eigenvalues yields a convenient way to assign the stopping partially to different contributions.

The slopes of the sum of all the expectation values belonging to one set of electrons of the same valence or semicore band are then analyzed in Table I. The main contribution for the stopping is given by $n = 3$ valence electrons. However, at large velocities, a considerable fraction is due to excitations of semicore ($n = 2$) electrons for the off-channeling trajectories. The calculated fractions are consistent with the results obtained from total stopping for the two different calculations with and without semicore electrons.

IV. HELIUM ATOM AND α PARTICLE AS PROJECTILE IN ALUMINUM

We now apply the framework that was discussed in the previous sections to the example of helium projectiles in aluminum (cf. Fig. 6). In test calculations we verified that the results for channeling projectiles again agree well for slow projectiles but underestimate the experimentally measured

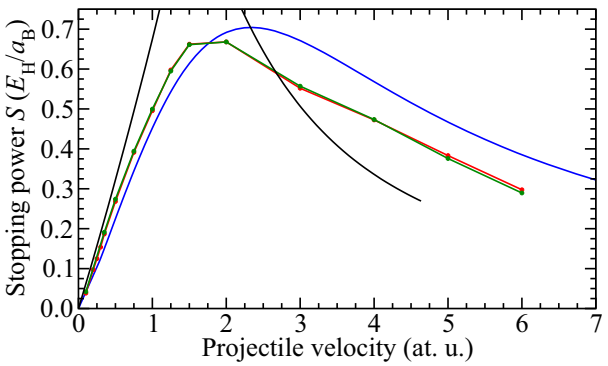

FIG. 6. (Color online) Electronic stopping calculated as a function of the velocity of a helium (solid red)/He^{2+} (solid green) projectile in aluminum under off-channeling conditions. The solid blue curve represents experimental results provided by the SRIM table [59]. The solid black curve is computed for a Lindhard dielectric function for three valence electrons per aluminum atom and a $Z_1 = 2$ projectile.

results for high projectile velocities (as in the case of the proton described before). Figure 6 shows that off-channeling projectiles in both charge states investigated here (neutral helium as well as alpha particles) experience the same electronic stopping. As can be seen in the same figure, our results also agree quite well with SRIM data [59]. Comparing these results to Fig. 3 shows that the electronic stopping of helium projectiles at low velocity is more than twice as large as for hydrogen projectiles (but not four times as expected by the linear response theory for $Z = 2$). We also confirm for helium projectiles that both semicore electrons and off-channeling trajectories are necessary to explain experimental results with this TDDFT approach.

In a recent experimental work [53], a change in the slope of the electronic stopping curve [see the dashed magenta curve in Fig. 5(b)] was observed, and this was interpreted as charge exchange processes between projectile and host. In a recent theoretical work [54], the authors did not find this feature for the stopping curve for their channeling projectiles, and they suggested that different impact parameters may be necessary to reproduce this feature. In our calculations, we did not observe this feature neither for the channeling nor off-channeling stopping curve. However, as in the case of hydrogen in aluminum, we find the electronic stopping of channeling projectiles to be smaller than the one for off-channeling ones. The apparent discrepancy might be reconciled if, due to some self-selection process, the relative importance of channeling trajectories is larger than that of off-channeling ones at low velocities in the experimental setup; which would be an effect that still can not be resolved in the length scale of our simulations. We note that the experimental data in Ref. [53] originates indeed from different experiments, and we suggest that those may correspond to different channeling geometries. Further experimental and theoretical work is necessary to clarify this point.

V. CONCLUSIONS

In summary, we establish a systematic framework for computing the electronic stopping power from the detailed atomistic description using first-principles Ehrenfest dynamics simulations based on real-time time-dependent density functional theory. These results are without any *a priori* assumption regarding the host environment (electron density, effective number of valence electrons, or dielectric function), or about the dynamic state of the projectile (ionization or charge state), and in general without any perturbative treatment. Our highly-scalable implementation of the fully first-principles approach [39,40] proves to be sufficiently efficient to allow simulations in large supercells (thousands of electrons) so that finite size effects are negligible, and it is also quantitatively accurate as demonstrated for the representative case of bulk aluminum for which detailed experimental data is available.

Our calculations show that off-channeling trajectories need to be taken into account to reproduce experimental results. This dependence on the trajectory arises from contributions to the electronic stopping due to strongly bound semicore electrons in aluminum atoms, and we proposed taking the geometrical/position average by setting the projectile direction

to be incommensurate with the crystal lattice vectors. We found that semicore electrons are particularly important for fast projectiles in the representative case of aluminum considered in this work. A large fraction of the semicore electrons participate in the off-channeling stopping, but not for channeling projectiles. Our results indicate great promise in applying the first-principles methodology for investigating important problems in materials under particle radiation, such as for understanding the role atomistic defects play in electron-ion energy transfer.

ACKNOWLEDGMENTS

We acknowledge fruitful discussions with E. Draeger, Y. Miyamoto, and A. Arnau. A.S. was supported through the Physical and Life Sciences Directorate at Lawrence Livermore National Laboratory. Computing support for this work came from the Lawrence Livermore National Laboratory Institutional Computing Grand Challenge program. Part of this work was performed under the auspices of the U.S. Department of Energy at Lawrence Livermore National Laboratory under Contract DE-AC52-07A27344.

[1] R. S. Averback and T. D. de la Rubia, Displacement damage in irradiated metals and semiconductors, Solid State Phys. **51**, 281 (1997).

[2] C. Race, *The Modelling of Radiation Damage in Metals Using Ehrenfest Dynamics*, Springer Theses (Springer, Berlin, Heidelberg, 2011).

[3] M. Toulemonde, C. Dufour, and E. Paumier, Transient thermal process after a high-energy heavy-ion irradiation of amorphous metals and semiconductors, Phys. Rev. B **46**, 14362 (1992).

[4] L. Mansur, Theory and experimental background on dimensional changes in irradiated alloys, J. Nucl. Mater. **216**, 97 (1994).

[5] G. Odette and B. D. Wirth, in *Handbook of Materials Modeling*, edited by S. Yip (Springer, Netherlands, 2005), pp. 999–1037.

[6] P. K. Patel, A. J. Mackinnon, M. H. Key, T. E. Cowan, M. E. Foord, M. Allen, D. F. Price, H. Ruhl, P. T. Springer, and R. Stephens, Isochoric heating of solid-density matter with an ultrafast proton beam, Phys. Rev. Lett. **91**, 125004 (2003).

[7] G. J. Caporaso, Y.-J. Chen, and S. E. Sampayan, The dielectric wall accelerator, Rev. Accel. Sci. Technol. **02**, 253 (2009).

[8] F. Komarov, A. Komarov, V. Pilko, and V. Pilko, Radiation resistance of structural materials of nuclear reactors on irradiation with high-energy hydrogen and Helium ions, J. Eng. Thermophys. **86**, 1481 (2013).

[9] T. D. de la Rubia, R. S. Averback, R. Benedek, and W. E. King, Role of thermal spikes in energetic displacement cascades, Phys. Rev. Lett. **59**, 1930 (1987).

[10] M. T. Robinson and I. M. Torrens, Computer simulation of atomic-displacement cascades in solids in the binary-collision approximation, Phys. Rev. B **9**, 5008 (1974).

[11] J. F. Ziegler, SRIM-2003, Nucl. Instrum. Meth. B **219–220**, 1027 (2004).

[12] S. Agostinelli, J. Allison, K. Amako, J. Apostolakis, H. Araujo, P. Arce, M. Asai, D. Axen, S. Banerjee, G. Barrand, F. Behner, L. Bellagamba, J. Boudreau, L. Broglia, A. Brunengo, H. Burkhardt, S. Chauvie, J. Chuma, R. Chytracek, G. Cooperman, G. Cosmo, P. Degtyarenko, A. Dell'Acqua, G. Depaola, D. Dietrich, R. Enami, A. Feliciello, C. Ferguson, H. Fesefeldt, G. Folger, F. Foppiano, A. Forti, S. Garelli, S. Giani, R. Giannitrapani, D. Gibin, J. G. Cadenas, I. González, G. G. Abril, G. Greeniaus, W. Greiner, V. Grichine, A. Grossheim, S. Guatelli, P. Gumplinger, R. Hamatsu, K. Hashimoto, H. Hasui, A. Heikkinen, A. Howard, V. Ivanchenko, A. Johnson, F. Jones, J. Kallenbach, N. Kanaya, M. Kawabata, Y. Kawabata, M. Kawaguti, S. Kelner, P. Kent, A. Kimura, T. Kodama, R. Kokoulin, M. Kossov, H. Kurashige, E. Lamanna, T. Lampén, V. Lara, V. Lefebure, F. Lei, M. Liendl, W. Lockman, F. Longo, S. Magni, M. Maire, E. Medernach, K. Minamimoto, P. M. de Freitas, Y. Morita, K. Murakami, M. Nagamatu, R. Nartallo, P. Nieminen, T. Nishimura, K. Ohtsubo, M. Okamura, S. O'Neale, Y. Oohata, K. Paech, J. Perl, A. Pfeiffer, M. Pia, F. Ranjard, A. Rybin, S. Sadilov, E. D. Salvo, G. Santin, T. Sasaki, N. Savvas, Y. Sawada, S. Scherer, S. Sei, V. Sirotenko, D. Smith, N. Starkov, H. Stoecker, J. Sulkimo, M. Takahata, S. Tanaka, E. Tcherniaev, E. S. Tehrani, M. Tropeano, P. Truscott, H. Uno, L. Urban, P. Urban, M. Verderi, A. Walkden, W. Wander, H. Weber, J. Wellisch, T. Wenaus, D. Williams, D. Wright, T. Yamada, H. Yoshida, and D. Zschiesche, Geant4-a simulation toolkit, Nucl. Instrum. Methods Phys. Res., Sect. A **506**, 250 (2003).

[13] E. Rutherford, LXXIX. The scattering of alpha and beta particles by matter and the structure of the atom, Philos. Mag. **21**, 669 (1911).

[14] J. Thomson, XLII. Ionization by moving electrified particles, Philos. Mag. **23**, 449 (1912).

[15] C. Darwin, XC. A theory of the absorption and scattering of the alpha rays, Philos. Mag. **23**, 901 (1912).

[16] H. Bethe, Zur Theorie des Durchgangs schneller Korpuskularstrahlen durch Materie, Ann. Phys. **397**, 325 (1930).

[17] P. Sigmund, *Particle Penetration and Radiation Effects*, Springer Series in Solid-State Sciences, Vol. 151 (Springer, Berlin, Heidelberg, 2006).

[18] R. Cabrera-Trujillo, J. R. Sabin, and J. Oddershede, Molecular stopping powers from the target oscillator strength distribution, Adv. Quantum Chem. **46**, 121 (2004).

[19] E. Fermi and E. Teller, The capture of negative mesotrons in matter, Phys. Rev. **72**, 399 (1947).

[20] J. Lindhard, M. Scharff, and H. E. Schiøtt, Range concepts and heavy ion ranges, Mat. Fys. Medd. Dan. Vid. Selsk. **33**, 1 (1963).

[21] J. Lindhard and A. Winther, Stopping power of electron gas and equipartition rule, Mat. Fys. Medd. Dan. Vid. Selsk. **34**, 1 (1964).

[22] I. Nagy, I. Aldazabal, and M. L. Glasser, The helium atom in metallic electron gases: A comparative study based on screened Schrödinger Hamiltonians, J. Phys. B: At. Mol. Opt. Phys. **45**, 095701 (2012).

[23] W. H. Barkas, J. N. Dyer, and H. H. Heckman, Resolution of the Sigma$^-$ Mass Anomaly, Phys. Rev. Lett. **11**, 26 (1963).

[24] P. M. Echenique, R. M. Nieminen, J. C. Ashley, and R. H. Ritchie, Nonlinear stopping power of an electron gas for slow ions, Phys. Rev. A **33**, 897 (1986).

[25] W. Kohn and L. J. Sham, Self-consistent equations including exchange and correlation effects, Phys. Rev. **140**, A1133 (1965).

[26] E. Runge and E. K. U. Gross, Density-functional theory for time-dependent systems, Phys. Rev. Lett. **52**, 997 (1984).

[27] M. Peñalba, A. Arnau, P. M. Echenique, F. Flores, and R. H. Ritchie, Stopping power for protons in aluminum, Europhys. Lett. **19**, 45 (1992).
[28] C. Race, D. Mason, M. Finnis, W. Foulkes, A. Horsfield, and A. Sutton, The treatment of electronic excitations in atomistic models of radiation damage in metals, Rep. Prog. Phys. **73**, 116501 (2010).
[29] D. Mason, J. le Page, C. Race, W. Foulkes, M. Finnis, and A. Sutton, Electronic damping of atomic dynamics in irradiation damage of metals, J. Phys.: Condens. Matter **19**, 436209 (2007).
[30] A. A. Correa, J. Kohanoff, E. Artacho, D. Sánchez-Portal, and A. Caro, Nonadiabatic forces in ion-solid interactions: The initial stages of radiation damage, Phys. Rev. Lett. **108**, 213201 (2012).
[31] Y. Miyamoto and H. Zhang, Electronic excitation in an Ar^{7+} ion traversing a graphene sheet: Molecular dynamics simulations, Phys. Rev. B **77**, 161402 (2008).
[32] S. Bubin, B. Wang, S. Pantelides, and K. Varga, Simulation of high-energy ion collisions with graphene fragments, Phys. Rev. B **85**, 235435 (2012).
[33] A. V. Krasheninnikov, Y. Miyamoto, and D. Tománek, Role of electronic excitations in ion collisions with carbon nanostructures, Phys. Rev. Lett. **99**, 016104 (2007).
[34] J. M. Pruneda, D. Sánchez-Portal, A. Arnau, J. I. Juaristi, and E. Artacho, Electronic stopping power in LiF from first principles, Phys. Rev. Lett. **99**, 235501 (2007).
[35] M. A. Zeb, J. Kohanoff, D. Sánchez-Portal, A. Arnau, J. I. Juaristi, and E. Artacho, Electronic stopping power in gold: The role of d electrons and the H/He anomaly, Phys. Rev. Lett. **108**, 225504 (2012).
[36] I. Tavernelli, M.-P. Gaigeot, R. Vuilleumier, C. Stia, M.-A. Hervé du Penhoat, and M.-F. Politis, Time-dependent density functional theory molecular dynamics simulations of liquid water radiolysis, Chem. Phys. Chem. **9**, 2099 (2008).
[37] A. Ojanperä, A. V. Krasheninnikov, and M. Puska, Electronic stopping power from first-principles calculations with account for core electron excitations and projectile ionization, Phys. Rev. B **89**, 035120 (2014).
[38] A. Tsolakidis, D. Sánchez-Portal, and R. M. Martin, Calculation of the optical response of atomic clusters using time-dependent density functional theory and local orbitals, Phys. Rev. B **66**, 235416 (2002).
[39] A. Schleife, E. W. Draeger, Y. Kanai, and A. A. Correa, Plane-wave pseudopotential implementation of explicit integrators for time-dependent Kohn-Sham equations in large-scale simulations, J. Chem. Phys. **137**, 22A546 (2012).
[40] A. Schleife, E. W. Draeger, V. M. Anisimov, A. A. Correa, and Y. Kanai, Quantum dynamics simulation of electrons in materials on high-performance computers, Comput. Sci. Eng. **16**, 54 (2014).
[41] V. Peuckert, A new approximation method for electron systems, J. Phys. C **11**, 4945 (1978).
[42] A. Zangwill and P. Soven, Density-functional approach to local-field effects in finite systems: Photoabsorption in the rare gases, Phys. Rev. A **21**, 1561 (1980).
[43] A. Zangwill and P. Soven, Resonant two-electron excitation in copper, Phys. Rev. B **24**, 4121 (1981).
[44] A. Zangwill and P. Soven, Resonant photoemission in barium and cerium, Phys. Rev. Lett. **45**, 204 (1980).
[45] A. Arnau, M. Pealba, P. Echenique, and F. Flores, A charge state approach to the stopping power of ions in solids, Nucl. Instrum. Meth. B **69**, 102 (1992).
[46] F. Gygi, Architecture of Qbox: A scalable first-principles molecular dynamics code, IBM J. Res. Dev. **52**, 137 (2008).
[47] See Supplemental Material at http://link.aps.org/supplemental/10.1103/PhysRevB.91.014306 for a more detailed analysis of computational aspects and convergence.
[48] G. Faussurier, C. Blancard, and M. Gauthier, Nuclear stopping power in warm and hot dense matter, Phys. Plasmas **20**, 012705 (2013).
[49] R. M. Martin, *Electronic Structure: Basic Theory and Practical Methods*, 1st ed. (Cambridge University Press, 2008), Vol. 1.
[50] For OPIUM pseudopotential generation program (including semi-core electrons), see http://opium.sourceforge.net
[51] N. Troullier and J. L. Martins, Efficient pseudopotentials for plane-wave calculations, Phys. Rev. B **43**, 1993 (1991).
[52] J. F. Ziegler, "SRIM-2003", http://www.srim.org/SRIM/SRIMPICS/STOP01/STOP0113.gif
[53] D. Primetzhofer, S. Rund, D. Roth, D. Goebl, and P. Bauer, Electronic excitations of slow ions in a free electron gas metal: Evidence for charge exchange effects, Phys. Rev. Lett. **107**, 163201 (2011).
[54] M. A. Zeb, J. Kohanoff, D. Sánchez-Portal, and E. Artacho, Electronic stopping power of H and He in Al and LiF from first principles, Nucl. Instrum. Meth. B **303**, 59 (2013).
[55] D. Blanchin, J.-C. Poizat, J. Remillieux, and A. Sarazin, Experimental determination of the energy loss of protons channeled through an aluminum single-crystal, Nucl. Instrum. Meth. **70**, 98 (1969).
[56] V. U. Nazarov, J. M. Pitarke, C. S. Kim, and Y. Takada, Time-dependent density-functional theory for the stopping power of an interacting electron gas for slow ions, Phys. Rev. B **71**, 121106 (2005).
[57] V. U. Nazarov, J. M. Pitarke, Y. Takada, G. Vignale, and Y.-C. Chang, Including nonlocality in the exchange-correlation kernel from time-dependent current density functional theory: Application to the stopping power of electron liquids, Phys. Rev. B **76**, 205103 (2007).
[58] V. U. Nazarov, J. M. Pitarke, Y. Takada, G. Vignale, and Y.-C. Chang, Time-dependent current-density functional theory for the friction of ions in an interacting electron gas, Int. J. Mod. Phys. B **22**, 3813 (2008).
[59] J. F. Ziegler, "SRIM-2003", http://www.srim.org/SRIM/SRIMPICS/STOP02/STOP0213.gif